

Fast exploration and learning of latent graphs with aliased observations

Miguel Lazaro-Gredilla¹, Ishan Deshpande¹, Sivaramakrishnan Swaminathan¹, Meet Dave¹ and Dileep George¹
¹DeepMind

Consider this scenario: an agent navigates a latent graph by performing actions that take it from one node to another. The chosen action determines the probability distribution over the next visited node. At each node, the agent receives an observation, but this observation is not unique, so it does not identify the node, making the problem *aliased*. The purpose of this work is to provide a policy that approximately maximizes exploration efficiency (i.e., how well the graph is recovered for a given exploration budget). In the unaliased case, we show improved performance w.r.t. state-of-the-art reinforcement learning baselines. For the aliased case we are not aware of suitable baselines and instead show faster recovery w.r.t. a random policy for a wide variety of topologies, and exponentially faster recovery than a random policy for challenging topologies. We dub the algorithm eFeX (from **e**fficient **e**xploration).

1. Introduction

We consider the problem of efficiently recovering latent graphs from aliased observations. To be precise, we try to recover, as accurately as possible, a latent graph from the observations of an agent that can move inside it, in as few steps as possible. At each step of the process, the agent is located at one of the nodes of the graph, and is free to choose which action to take. Each action has a distribution over which nodes the agent will travel to when performing the action (including staying in the same node, which corresponds to a self-loop in the graph). At each node, the agent can observe the node’s label, which is fixed. Multiple nodes can have the same label, i.e., the graph is *aliased*. This prevents the agent from identifying the node in which it is located from the observation, and also has no knowledge about which edges are present in the graph (i.e., does not know how actions make it transition to other nodes). This makes the graph *latent*. The graph is technically a *directed multigraph*, because edges are specific to actions, and two or more actions can connect the same pair of nodes, in the same or different directions.

The aim of the agent is two-fold: (a) use the collected observations so far (which will be observation-action pairs) to recover the latent graph that it is traversing as accurately as possi-

ble; and (b) to follow a policy that allows it to gather information as quickly as possible to improve the accuracy of recovery. Previous work in latent graph recovery has mostly been focused on the unaliased case. [George et al. \(2021\)](#) consider the aliased case, but ignore the problem of efficient exploration and default to a random policy. In this work we tackle both problems simultaneously since they complement each other: modeling the environment is helpful to better explore it (e.g., avoiding revisiting the same area of the graph, or getting stuck in densely connected areas with few connections to other parts of the graph), and better exploring the environment helps to better recover its topology for any given budget of steps.

Our proposal, called **e**fficient **e**xploration (eFeX) for obvious reasons, builds on top of the clone-structured causal graphs (CSCGs) from [George et al. \(2021\)](#). CSCGs are a computational model for the hippocampus —similar in philosophy to the Tolman-Eichenbaum machine [Whittington et al. \(2020\)](#)— that can recover structure from sequences. Structure from multiple domains can be handled, including conceptual, spatial, and others. Here we focus on spatial navigation. The present work endows CSCGs with a policy for fast exploration. CSCGs are a probabilistic white-box graphical model, meaning that we recover an explicit, approximate graph of the environment

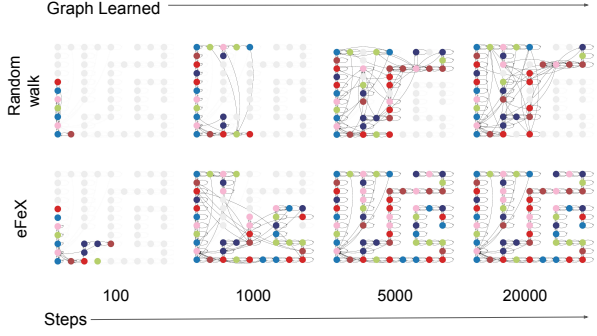


Figure 1 | An agent explores a latent graph G' and receives aliased observations, from which it creates a “mental model” G (pictured) of it. Using G to inform exploration makes eFeX explore more efficiently, covering more ground and recovering a better model.

that the agent “lives” in. This is particularly convenient because it enables several downstream tasks: graph manipulation (see, e.g. [Tong et al., 2012](#)), latent node recovery from observations, planning in the graph (including hierarchical variants), etc. Most probabilistic queries are exact, see [George et al. \(2021\)](#).

Fast exploration is particularly important in real-world settings in which exploring the environment is costly in terms of time, energy, etc. Another field in which fast exploration is relevant is reinforcement learning (RL), see e.g. the Memory&Planning game and One-shot StreetLearn discussed in [Ritter et al. \(2020\)](#), or the chain environment from [Osband et al. \(2016\)](#); [Shyam et al. \(2019\)](#). In RL, agents maximize cumulative reward, but sometimes fail to even discover states of high reward if the topology to explore is challenging and/or the step budget is limited. Reward shaping is a mechanism to mitigate this, but it is not very scalable, since it often requires expert human design per environment type. With eFeX we introduce a new intrinsic reward that simply pursues obtaining a better model of the environment. See [Amin et al. \(2021\)](#); [Yang et al. \(2021\)](#) for a detailed review of efficient exploration in the context of RL.

The contributions of eFeX are as follows:

- Recovery of an *explicit graph* of the environment from *aliased* observations. Prior work

only handled the unaliased case, and often did not produce a graph.

- Development of an information-theoretic policy for fast exploration on top of CSCGs ([George et al., 2021](#)) that can be computed in closed form, while prior work ([Shyam et al., 2019](#)) relied on approximations.
- Exponentially faster than a random policy for challenging, aliased graph topologies. In the simpler, unaliased setting where baselines exist, recovery is still faster when using eFeX.
- Works for arbitrary graphs, i.e., does not make topological assumptions, Euclidean or otherwise. Action meaning is arbitrary and can be different for each node.
- Depends only on three easy-to-tune parameters.

The rest of this paper is organized as follows. In Section 2 we define the problem to solve in precise mathematical terms and introduce the notation that we will be using through the rest of the paper; we develop the probabilistic model and the information-theoretic foundations of the fast exploration policy of eFeX along with its complete algorithmic description in Section 3; we discuss its connections with related work in Section 4; we empirically verify its performance w.r.t. both existing deep learning-based baselines and random policies in Section 5; finally, we conclude the paper with a discussion of our findings in Section 6.

2. Problem set-up

Consider a directed latent graph G that an agent can traverse by performing actions. At any given time step n , the agent is located at a node of G , and receives an observation x_n from it. Multiple nodes can produce the same observation (i.e., they are *aliased*), and hence the location in the graph is not determined by the observation. Then, the agent performs an action a_n , traverses one of the outgoing edges from that node with that action label, and lands at the target node of that edge in G . All the edges of the graph, in addition to being labeled with an action, have an associated probability, and the probabilities of all the edges leaving from the same node with

the same action label sum up to one. Edges with probability zero are not present in the graph.

Several clarifying observations are in order. First, the actions are defined per node, so their number and meaning (which is unknown to the agent) can change from node to node. Second, in the simplest case, in which only one action is available at all nodes, G is a standard directed graph, edges only need to be annotated with a probability (and not with an action), and all that the agent gets is a stream of observations, x_1, \dots, x_N . However, in the case in which multiple actions are available, G becomes a directed multigraph, since two directed edges with the same source and target (but annotated with different actions) might appear. In this case, edges are annotated with both an action and a probability, and the agent will receive a stream of observation-action pairs $x_1, a_1, \dots, x_N, a_N$.

To precisely define a graph, we use the tensor T and the matrix E , so $G \equiv \{T, E\}$. T defines the action-conditional transitions, so $[T]_{ijk} = P(z_{n+1} = k | z_n = j, a_n = i) \forall_n$, where z_n is the latent state at time step n (i.e., the node of the graph at which the agent is located, which cannot be observed), and a_n is the action taken by the agent to move from node z_n to node z_{n+1} . E defines the observations emitted at each of the nodes, and it is a binary matrix obtained by stacking the one-hot encodings of the observations emitted at each node. One way to write this is to say that $[E]_{ij} = P(x_n = j | z_n = i) \forall_n$, where x_n is the observation that the agent receives from the node visited at time step n , which is z_n . The probability distribution is actually *deterministic*, i.e., zero for all values of x_n except one. This means that a node always emits the same observation. The transition tensor and emission matrix do not depend on n . For an example of a graph G and its corresponding transition T and emission E , see Appendix A.

All the nodes (latent states) that emit the same observation are aliased because they can not be disambiguated by their emission alone, and the agent needs to rely on context. Aliased nodes are called *clones* and their set for a given observation x is denoted by $C(x)$. In a graph G , the probability of a stream of observations x_1, \dots, x_N , given the

action sequence a_1, \dots, a_N that the agent chooses to take is

$$P(\mathbf{x} | \mathbf{a}, G) = P(x_1, \dots, x_N | a_1, \dots, a_N, G) = \quad (1)$$

$$\sum_{z_1 \in C(x_1)} \dots \sum_{z_N \in C(x_N)} P_G(z_1) \prod_{n=1}^{N-1} P(z_{n+1} | z_n, a_n),$$

which can be computed efficiently by performing the summations and multiplications in the right order. It is, in fact, an action-conditional version of a hidden Markov model (HMM) with a known, deterministic emission matrix, and thus enjoys the same tractability. For more details, see previous work on CSCGs (George et al., 2021).

The problem is to devise an agent that, by taking the appropriate sequence of actions on a ground truth graph G' , recovers a graph G as close as possible to G' in as few steps as possible. This process is visualized in Fig. 1.

2.1. Measuring the quality of a solution

To properly specify the latent graph recovery problem, we need to provide a quantitative measure of the quality of an agent's solution. We will refer to the ground-truth graph as G' and to the agent's recovered graph as G . Then we define the expected log-likelihood of G under G' as

$$\mathcal{L}_{G'}(G) = \lim_{N \rightarrow \infty} \mathbb{E}_{\mathbf{a} \sim U} \left[\sum_{x_1, \dots, x_N} P(\mathbf{x} | \mathbf{a}, G') \log P(\mathbf{x} | \mathbf{a}, G) \right],$$

where U generates sequences by sampling from the uniform distribution over the available actions at each time step, i.e., uses a random policy. This measure is always negative, and higher is better. A value of $\mathcal{L}_{G'}(G) = 0$ can only be achieved when G is perfectly recovered and actions have deterministic results. In general, $\mathcal{L}_{G'}(G) \leq \mathcal{L}_{G'}(G')$, and reaching the upper bound implies perfect recovery.

Observe that this definition has a very convenient property: an agent traversing the environment taking a random action at each time step can get an arbitrarily good approximation to $\mathcal{L}_{G'}(G)$ by traversing the graph for long enough and with enough restarts. I.e., access to the true T' and E' , or to the true latent state of the graph during traversal, is not necessary to compute a good approximation.

2.2. Degenerate solutions

Given that for a given ground truth G' perfect recovery results in $\mathcal{L}_{G'}(G) = \mathcal{L}_{G'}(G')$, one might (incorrectly) assume that $\mathcal{L}_{G'}(G) = \mathcal{L}_{G'}(G')$ implies that $G = G'$. This is not true, and multiple degenerate solutions with the same expected log-likelihood can be obtained. Two mechanisms are at play in this degeneracy:

Node relabeling Given a ground truth graph G' , an isomorphic graph can be obtained by relabeling its nodes. If G' and G are isomorphic, then $\mathcal{L}_{G'}(G) = \mathcal{L}_{G'}(G')$. This is the only mechanism for degeneracy in the simple case in which both the original and degenerate graph have no aliasing (i.e., each node emits a unique observation) and a single action is available (i.e., actions are irrelevant). With those conditions, G' and G are isomorphic if and only if $\mathcal{L}_{G'}(G) = \mathcal{L}_{G'}(G')$.

Clone merging and splitting In graphs in which aliasing is permitted, it is possible to split a node into two clones of the same node with the same incoming and outgoing edges, and this operation can also be reversed (merging). If only merging and splitting operations are performed on a ground truth graph G' , the obtained graph G will have $\mathcal{L}_{G'}(G) = \mathcal{L}_{G'}(G')$. See Appendix A for an example.

Since the agent has no way to tell apart degenerate solutions (e.g., an isomorphism) from the actual ground truth, and since a degenerate solution G for which $\mathcal{L}_{G'}(G) = \mathcal{L}_{G'}(G')$ is, for most practical purposes, just as useful as having access to G' , we regard all solutions with the same $\mathcal{L}_{G'}(G)$ as equally good solutions.

3. Method

Given a sequence of observation-action pairs, G' can be approximately recovered by maximizing Eq. (1), i.e., maximum likelihood. However, it begs the question of how to obtain that sequence in the first place. The naive approach would be for the agent to take an action at random from those available at each node. However, that might not be the fastest way (in terms of the number of

steps) to obtain a model G of a given quality (i.e., of large enough $\mathcal{L}_{G'}(G)$).

3.1. Model-based active exploration

To explore more efficiently, an agent can keep at each step an internal belief (posterior) over G , based on the observation-action pairs seen so far. Then it can evaluate, based on its current belief, how informative each potential action would be. Finally, it should take the most informative action.

Let us consider single actions first. Let us say that an agent is at node z , it takes action a , and lands at node z' . How informative is that specific transition? Using the definition of information gain, we have that

$$\text{IG}(a, z, z') = \text{KL}(p(T|a, z, z') || p(T)),$$

where we are ignoring E , since we will consider it constant and known (more on this later). The above definition cannot be used directly, since when the agent is at z , it needs to decide which action a to take, but it does not know yet where it will land. Instead, we will take its expectation w.r.t. z' , and additionally marginalize out the transition tensor T according to the current beliefs of the agent. Thus, we define the utility of action a at node z as

$$u(z, a) = \int_T \sum_{z'} \text{IG}(a, z, z') P(z'|z, a, T) p(T) dT,$$

which can also be expressed (Shyam et al., 2019) as

$$u(z, a) = \text{JSD}\{P(z'|z, a, T) | T \sim p(T)\},$$

i.e., the Jensen-Shannon divergence among the (infinitely many) distributions $P(z'|z, a, T)$ that can be obtained when sampling from the current belief $p(T)$. This initial definition of utility is identical to the one in Shyam et al. (2019) and has the same motivation. In contrast with that work, we will be able to find a closed-form expression for $u(z, a)$, as opposed to a sampling approximation that requires training a separate neural network (NN) per sample.

3.1.1. Exact utility computation

Let us consider the unaliased case first (which incidentally is the only case considered by most

of the relevant literature, and in particular, by [Shyam et al. \(2019\)](#)). This allows us (up to an irrelevant node relabeling), to set the emission matrix to the identity $E = I$, and therefore directly observe the node identities z_n .

Now, we slice the 3D transition tensor T in “rows”. In particular, for a given node z and action a , the corresponding entries of T form a non-negative vector t_{az} that sums up to one. This vector defines a categorical distribution over the nodes of the graph. We can place a conjugate, symmetric Dirichlet prior with parameter α over this distribution, $t_{az} \sim \text{Dir}(\alpha)$. I.e., $p(t_{az})$ is a distribution over distributions. The posterior after observing one or more transitions from node z and under action a is also Dirichlet, so we can keep our belief $p(t_{az})$ conveniently parameterized as a Dirichlet distribution at all times. More precisely, we will keep a “counts” vector c_{az} with one entry per destination z' . It will store the number of times that we have transitioned from z with action a to each possible destination node. Then, the belief of the agent (posterior) after observing all past transitions, over the transition tensor will be $p(T|\mathcal{D}_N) = \prod_{az} p(t_{az}|\mathcal{D}_N)$, with $p(t_{az}|\mathcal{D}_N) = \text{Dir}(c_{az} + \alpha) = \text{Dir}(b_{az})$, where $\mathcal{D}_N \equiv x_1, a_1, \dots, x_N, a_N$, and $b_{az} \triangleq c_{az} + \alpha$. Observe that c_{az} can be computed trivially from \mathcal{D}_N , since for $E = I$, $z_n = x_n$ and c_{az} are simply counts of observed transitions $z \xrightarrow{a} z'$. This results in the closed-form utility function

$$\begin{aligned} u(z, a) &= \text{JSD}\{P(z'|z, a, t_{az})|t_{az} \sim \text{Dir}(b_{az})\} \\ &= H(\mathbb{E}_{t_{az} \sim \text{Dir}(b_{az})}[t_{az}]) - \mathbb{E}_{t_{az} \sim \text{Dir}(b_{az})}[H(t_{az})] \\ &= H\left(\frac{b_{az}}{1^\top b_{az}}\right) + \left(\frac{1^\top (b_{az} \odot \psi(b_{az} + 1))}{1^\top b_{az}}\right) \\ &\quad - \psi(1^\top b_{az} + 1), \end{aligned} \quad (2)$$

which is one of the main results of this paper. $H(\cdot)$ is the entropy function, $\psi(\cdot)$ is the digamma function, \odot is the elementwise product of two vectors, and 1^\top is a row vector of ones of the appropriate length. Details of the derivation are provided in [Appendix E](#). Thus, if we were to only take one action, and we were located at node z , we should take action $\arg \max_a u(z, a)$, which we can compute exactly given the cumulative action-conditional observed transitions (stored in c_{az}). Doing so would maximize the information

gain and thus maximally shrink our belief $p(T)$, making our current estimate of G as precise as possible in a single step.

3.2. Reinforcement learning for active exploration

The above analysis attributes a utility (a one-step information gain) to each node-action pair. When more than one action can be taken, simply following the one-step maximum information gain may not result in the best total information gain. For instance, a very large utility might appear two steps away from the agent’s location, but the local utility of the first step might guide the agent away from it.

Computing the multistep information gain would be very involved and computationally infeasible above a few steps. Instead, we can use the utility as a local reward and obtain a global policy from it by casting the problem as standard reinforcement learning (using some discount factor γ). This would be exact if the utility did not change as the agent traverses the graph. However, as the agent traverses the graph, it captures more information about it, and the utility changes. Therefore, the approximation here is that the utility does not change rapidly as the agent traverses the graph.

In reinforcement learning terms, we are looking for an optimal policy, which can be obtained using value iteration. Since the utility changes at each step, we should also recompute the policy at each step. If the utility is assumed to evolve slowly enough, one can recompute the policy only every few steps to reduce computational effort. A practical recommendation to speed up convergence is to initialize value iteration with the result from the previous step.

Value iteration requires an action-conditional transition matrix \bar{T} , but at any point in time the agent is holding a whole belief $p(T)$ for it, instead of a single point estimate. A simple solution is to set it to its expectation, i.e., use $[\bar{T}]_{az} = \bar{t}_{az} \triangleq \mathbb{E}_{t_{az} \sim \text{Dir}(b_{az})}[t_{az}] = b_{az}/1^\top b_{az}, \forall_n$.

Observe that this approach, in contrast with the approach taken by [Shyam et al. \(2019\)](#), would

provide the optimal action sequence if the utility did not change at each step. Also, rather than a (stochastic) Monte Carlo tree search, it uses the deterministic, globally convergent value iteration.

3.3. Extension to the aliased case

So far we have described a complete algorithm for fast exploration in unaliased environments. The only input that it needs is the count vectors c_{az} , \forall_{az} . These vectors simply record the experienced transitions in the latent space.

When working with a (potentially) aliased graph, we can reuse that machinery as long as we are able to produce an approximate decoding of the hidden states z_n that the agent visits, which now will be distinct from the observation x_n .

To do this, first we allocate several clones to each observation. In practice, this means that we hardcode an emission matrix E , allocating multiple hidden states to the same observation, even before the agent starts traversing the graph (see Fig. 4(b) in Appendix A, for an example E where 2 clones are assigned to each observation). E will have size $n_E \times n_H$, where n_E is the number of distinct observations and $n_H \geq n_E$ is the number of latent states. Once E is known and fixed, we can use Eq. (1) to compute the likelihood of the transition tensor T , given the sequence of observation-action pairs. Furthermore, we can use expectation-maximization (EM) to maximize the likelihood of T given the observed data so far, \mathcal{D}_N . In fact, running EM to optimize Eq. (1) is identical to running EM to learn an HMM¹, since both have the same structure, but it can be coded in a computationally more efficient way, because of the high sparsity of the hardcoded emission matrix E . Once T has been estimated, one can use Viterbi decoding to turn the observation sequence x_1, \dots, x_N into an estimated sequence of hidden states $\hat{z}_1, \dots, \hat{z}_N$.

Now the hidden state sequence can be used, as if we were in the unaliased case, to compute the count vectors c_{az} , follow the previous procedure,

¹This model falls within the class of *overcomplete HMMs*, which are known to have favorable properties for learning when the transition matrix is highly sparse and does not contain probable short cycles (Sharan et al., 2017).

and ultimately decide on the next approximately best action. Putting everything together, we obtain the eFeX algorithm. Complete pseudocode is provided in Appendix B.

4. Related work

The proposed eFeX algorithm has three fundamental characteristics: (a) it favors efficient exploration; (b) it handles aliased observations; and (c) it recovers an explicit graph of the environment dynamics, from which it can effectively dealias the observation sequence into an estimated hidden state sequence. We now contrast eFeX with existing work.

The exploration problem² in RL is discussed at length in the survey papers Amin et al. (2021) and Yang et al. (2021), where various possible guiding principles for exploration are analyzed. In these works, exploration is traded off with exploitation, i.e., unlike in eFeX—which only explores to better recover a model of the environment—exploration coexists with capturing the (sparse) reward of a RL task. Also unlike eFeX, the discussed works cannot handle aliasing. Ecoffet et al. (2021) introduces the Go-Explore family of algorithms and shows significantly improved performance in Atari games (particularly Montezuma Revenge and Pitfall). The Go-Explore policy is qualitatively similar to eFeX in that it results in a frontier of nodes that are insufficiently explored to which the algorithm learns to “Go” and from which it launches new “Explore” actions. However, its operation regime is almost the opposite of eFeX w.r.t. aliasing: the state (pixels on screen) is fully observed, but it is down-sampled (purposefully introducing aliasing) to reduce its size, and the modeling is done directly in this aliased space. Most works use model-free deep RL (Bellemare et al., 2016; Osband et al., 2016; Ritter et al., 2020), and do not discover the explicit latent graph that describes the environment. Machado

²Before becoming connected with RL, works on exploration made insightful observations. Wilf (1989) poses the “white screen problem”. i.e., how long it takes for a random walk on the 2D grid of a computer screen to visit all its pixels. The author noted that while exploration proceeds fast at the beginning, visiting the last few pixels in the screen takes much longer.

et al. (2017a,b) do not directly tackle exploration, but simplify it by aggregating actions into *options*. Dai et al. (2019) uses an explicit, ground truth, graph of the environment, which is fully revealed to the agent either a priori or as it traverses the environment, but is not learned from noisy or aliased observations. Shyam et al. (2019) propose model-based active eXploration (MAX). MAX discovers a model of the transitions of the environment, modeled as an ensemble of deep NNs, and uses the information gain principle to guide exploration. This work is the closest to eFeX.

Both MAX and eFeX are guided by the same information gain principle, but there are fundamental differences in how it is computed and used. First, their utility function, defined in (Shyam et al., 2019, Eq. 8), is approximated via sampling over deep NNs, whereas we obtain a closed form solution, Eq. (2). Second, for each sample in the approximation, a new deep NN needs to be trained, which makes it more computationally demanding than simply evaluating Eq. (2). To limit computational effort, Shyam et al. (2019) use a very small number of samples, thereby obtaining a coarse approximation of the utility. Finally, we use value iteration to globally propagate the local utility, whereas (Shyam et al., 2019) uses Monte Carlo tree search, which can limit the performance of their method in the case of distant utilities.

In contrast with the above methods, CSCGs (and therefore eFeX) can handle aliasing. They create a higher-order network Lambotte et al. (2019); Xu et al. (2016) using cloning. Aliasing has been considered in previous works. Whitehead and Ballard (1991) introduced the problem of “perceptual aliasing”, although not in the context of exploration. However, their take is that aliasing can be harmful or beneficial, depending on whether it conflates states that are actually equivalent for the task at hand or not. We saw above that Ecoffet et al. (2021) purposefully introduce aliasing in their data to their benefit. Therefore, their approach is aimed at introducing “the right type of aliasing for the task”. This is only possible in the case in which raw data is unaliased to begin with, as it is the case in Ecoffet et al. (2021). In contrast, eFeX handles aliasing

that is present in raw data and therefore cannot be tuned for the task at hand. McCallum (1996) attempts to handle aliasing by augmenting each state with the last few states in the sequence, using a memory length that is dynamically determined. Although this can handle certain types of aliasing, it is fundamentally limited (through the use of clones, eFeX can theoretically handle aliasing that would require an arbitrarily long amount of memory). Also note that the state space grows exponentially with the length of the used memory. Building up on that work Shani and Brafman (2004) propose a mechanism to handle the case in which the observations at each state are not deterministic, but stochastic. Although we do not consider that setting in the present work, it is easy to see that it would correspond to a modification in eFeX in which the emission matrix would no longer be fixed a priori, but would have to be learned instead.

5. Experiments

In this section we will evaluate the performance of eFeX (Algorithm 1, see Appendix B) in multiple settings. After discussing performance measures in Subsection 5.1, we consider the case of non-aliased graphs in Subsection 5.2. Because this simpler problem has been previously addressed in the literature, we can establish a direct comparison with existing methods. Then, in Subsection 5.3 we will introduce aliasing in a particularly challenging topology that tends to resist exploration, and show that eFeX is exponentially faster than a random policy, since we are not aware of pre-existing work applicable in the aliased setting. Finally, in Subsection 5.4 we compare eFeX with a random policy on a variety of topologies.

One of the free parameters of eFeX is the number of clones allocated to each observation. This number should simply be “large enough”, and in fact, matching the number of ground truth clones, while theoretically enough, results in EM struggling to find good optima. The benefits of overparameterization when learning latent variable models is a previously studied phenomenon, see Buhai et al. (2020), and particularly in the case of EM learning, see Xu et al. (2018). We

allocate the same number of clones to all observations, which, unless specified otherwise, are selected to be (on average) twice as many as the ground truth ones. The two remaining eFeX parameters are set to $\alpha = 2 \times 10^{-4}$ and $\gamma = 0.9999$. We use this parameterization for all our experiments, since we observed that further fine-tuning had very little impact on the results.

5.1. Measuring performance

When comparing multiple methods for efficient latent graph recovery, we want to know both (a) how fast (in terms of exploration steps, not computational performance) we recover the latent graph; and (b) how well we recover the graph. This is best shown through a plot of performance vs. number of steps in the unknown environment.

In unaliased, deterministic environments, we can measure the *coverage* of the exploration by counting the fraction of transitions explored. This gives an intuitive idea of both the speed and quality of the recovery. However, in the aliased stochastic setting that we are interested in, the coverage is ill-defined, and a more complete measure is the expected log-likelihood $\mathcal{L}_{G'}(G)$ defined in Section 2.1. We will report either as appropriate for each experiment.

In Appendix C we generalize *coverage* to the aliased stochastic setting and introduce a complementary *precision* measure. These are reported Appendix F.

5.2. Non-aliased graphs

We consider here the chain graph environment from Shyam et al. (2019) depicted in Fig. 2 (top). It was posed originally in Osband et al. (2016) as a simplification of the “River Swim” problem from Strehl and Littman (2008). The environment consists of a chain of L nodes, each emitting a unique observation. I.e., this is an unaliased problem that corresponds to one-clone-per-observation in eFeX, or, equivalently, to the emission matrix being the identity matrix, $E = I$. Each node has two outgoing edges connecting it to their neighbors. What makes it tricky is that the labels of those edges (the actions that traverse them, noted as L and R

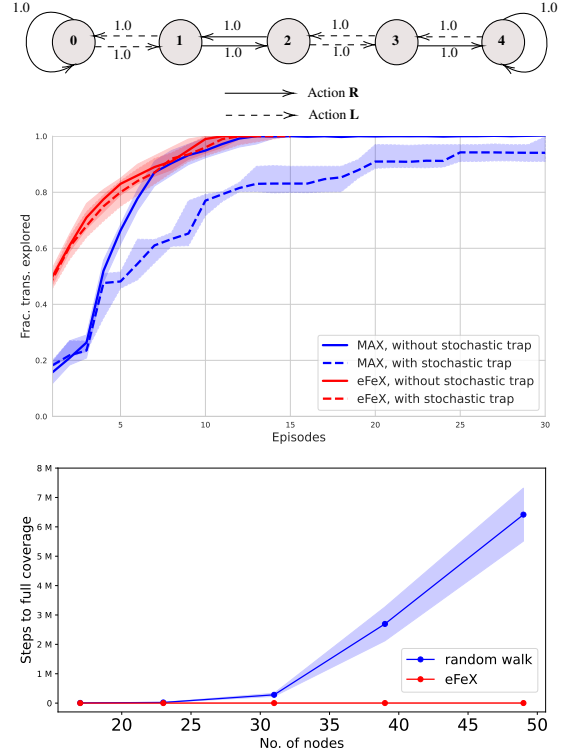


Figure 2 | Top: chain for $L = 5$. Middle: coverage for $L = 50$. The stochastic trap barely affects the performance of eFeX. Bottom: Scaling with the size of the “maze” topology, under the random and eFeX policies. eFeX is exponentially more efficient. Averaged over 100 runs. 95% confidence intervals provided.

in Fig. 2 (top)) are randomly flipped along the chain, so that a trivial policy that just repeats the same action will not traverse the full chain, but instead become trapped in a loop in a local region. Instead, the policy has to be smart enough to take different actions at each node to keep exploring new nodes. The end nodes of the chain only have one neighbor, so the other action will simply be a self-loop. Instead of a single uninterrupted walk, the problem is posed as a sequence of episodes of length $L + 9$, with the agent starting each episode at the node labeled as “1”. This means that there are few actions to spare within an episode if the agent wants to achieve full exploration, and that any progress towards the right will be undone at the beginning of each episode, so exploration has to be very deliberate to succeed.

A harder variant of this problem introduced in

[Shyam et al. \(2019\)](#) incorporates a “stochastic trap” at node “0”: both the L and R actions will remain in node “0” or transition to state “1” with probability 0.5 (not pictured). The purpose of the stochastic trap, as the authors explain, is to trick models that conflate *risk* (unlearnable unknowns) with *uncertainty* (learnable unknowns). Such models will be lured by the randomness of results experienced at node “0”, thinking it is uncertainty, and that they should keep exploring it to reduce it, when it is actually unavoidable risk. Thus, such models will make little progress in exploring the rest of the chain.

We compare the performance of eFeX with the model-based active exploration from [Shyam et al. \(2019\)](#), called MAX, which in turn beats deep Q-network (DQN) approaches such as exploration bonus DQN ([Bellemare et al., 2016](#)) and bootstrapped DQN ([Osband et al., 2016](#)). As shown in Fig. 2 (middle), without stochastic trap, MAX only needs 18 episodes (including 3 episodes of warm-up time) for exploring all the transitions in a 50-state chain (much fewer than deep Q-learning, not shown here). But eFeX is faster, only needing 11 in the median case. The gap becomes much larger once the stochastic trap is activated, with eFeX barely slowing down. This also shows that eFeX, like MAX, is not conflating risk and uncertainty. The superiority of eFeX over both deep Q-learning and MAX is not surprising given that MAX beats deep Q-learning and eFeX improves over MAX in terms of utility computation and propagation (see Sections 3 and 4).

5.3. Aliased graphs

Now we move to environments that contain aliasing, i.e., the observations do not unambiguously identify the node of the graph that the agent is at. We will quantify the degree of aliasing of an environment by the *unique fraction*, $UF = \frac{\# \text{ unique observations in } G'}{\# \text{ nodes in } G'}$. No aliasing corresponds to $UF = 1$, and as this figure reduces, aliasing becomes more severe, and recovery is harder.

We consider a “maze” topology, as depicted in Figure 3 (bottom-right), made up of adjacent cells that the agent can traverse. At each cell, the color is provided to the agent as an observation.

Observe that colors repeat in multiple cells: we design this environment to be highly aliased, with $UF = 0.1$. At each cell the agent can take one of four actions (up, down, left, right) to travel to the adjacent cell. However, in 90% of the cases in which there is no adjacent cell, the graph will contain a self-loop, so the agent remains in place. For the remaining 10% of cases, the graph contains an edge that will transport the agent back to a designated “home” node (arbitrarily chosen, but fixed). A very deliberate policy is required for the agent exploring nodes far from home.

Since existing works like MAX or deep Q-learning are not applicable here due to aliasing, we compare the performance of eFeX with that of a random policy. Figure 2 (bottom) shows the number of steps required to explore the whole environment for each size, and show that eFeX is exponentially more efficient as the size grows. As a concrete data point, a maze with 59 states is fully explored by eFeX in 5,000 steps, whereas the random walk is unable to fully explore it even after 20,000 steps.

5.4. Aliased graphs, multiple topologies

Finally, to test the generality of eFeX, we run it on a variety of challenging topologies with severe aliasing ($UF = 0.1$) and *slippage*. Slippage makes navigation more realistic by making the results of actions stochastic. In particular, when a basic action such as `left` is executed, the environment executes it k times, with $P(k) = (1 - P_{\text{slip}})P_{\text{slip}}^{k-1}$, $k \geq 1$. We set $P_{\text{slip}} = 0.1$, so that when we execute e.g. `left`, the agent moves left once only 90% of the time, slipping further in the remaining cases, following the specified geometric distribution. This makes the environment more challenging to learn. The agent has no access to the amount of slippage that has occurred, just to the observation, as always, which due to aliasing will not resolve the amount of slippage either.

The topologies that we will be testing are shown in Figure 3 (bottom), with each color representing a different observation. Details are provided in Appendix D.

Here we report expected log-likelihoods for the

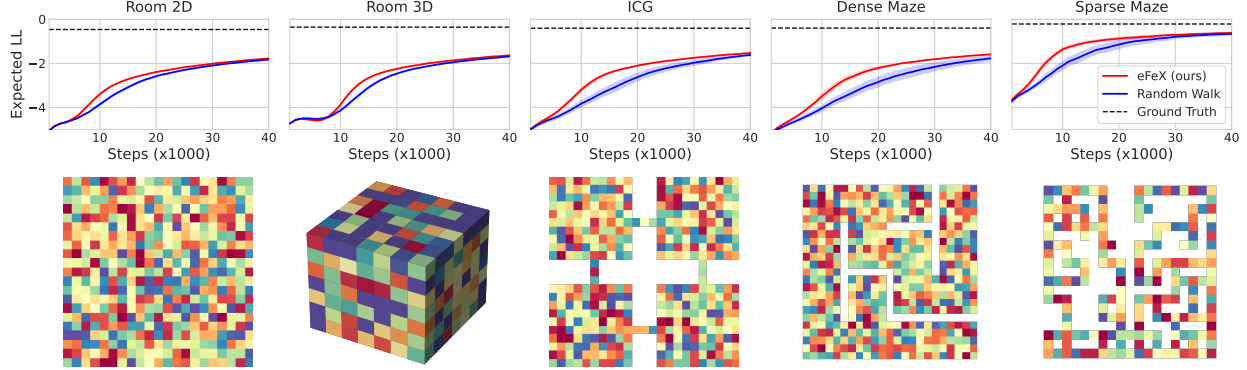


Figure 3 | Top: Expected log-likelihood for each topology, as a function of the number of steps of the agent in the environment. Higher is better. Results are averaged over 100 runs. Bands indicate 95% confidence intervals for the averages. Random policy shown in blue, eFeX in red. Environment parameters $UF = 0.1$ and $P_{\text{slip}} = 0.1$. Bottom: Exploration environments. Colored locations are accessible, and white regions are inaccessible. The colors represent the (categorical) observation that the agent receives at each location.

different topologies with $UF = 0.1$ and $P_{\text{slip}} = 0.1$. More complete measures (see Appendix C) for this and other parameterizations are provided in Appendix F. As expected, eFeX performs better than a random policy in the ICG and the mazes, w.r.t. all measures. Somewhat surprisingly, it also beats the random policy in the regular grids, although with a smaller advantage. Looking at the weighted coverage and precision measures (Appendix F.9), it seems like between 30,000 and 50,000 steps (depending on the topology) are sufficient for recovering a surrogate graph G that can be mapped back almost perfectly to the ground truth G' .

6. Discussion

In this work we have introduced eFeX, an algorithm for fast exploration and recovery of aliased latent graphs. When working in the simpler setting in which graphs are unaliased, we can establish direct comparisons with recent, state-of-the-art algorithms, such as the model-based MAX (Shyam et al., 2019) or the deep-Q-learning-based exploration bonus DQN (Bellemare et al., 2016) and bootstrapped DQN (Osband et al., 2016). These baselines are outperformed by eFeX.

In the aliased regime, eFeX is, to the best of our knowledge, the first algorithm able to recover

the latent graph through the use of an active policy aimed at minimizing the number of steps in the environment. We show empirically that when the topology becomes challenging, eFeX can be exponentially better than a random policy. As shown in Appendix F, both aliasing and stochasticity reduce the speed at which we can recover a latent graph, since the problem is harder. But eFeX does not break as we introduce aliasing and stochasticity, instead degrading gracefully.

Framing fast exploration as latent graph recovery means that we get some additional benefits when running eFeX: the resulting model is a directed multigraph representing the environment, which is easily inspectable and modifiable. The model is probabilistic and generative, so it can be used as a surrogate of the environment and can also answer arbitrary probabilistic queries, which enables new functionalities: from counterfactuals, to planning, to filtering or smoothing given partial observations. Given the simplicity of the model, all these queries are tractable.

We expect eFeX to find practical applications in RL, where agents need to efficiently discover high-reward states. If rewards are sparse enough, the agent might not have much guidance as to how to find them, so designers often need to resort to reward shaping, which in turn tends to involve manual tuning. In contrast, model-based active exploration builds a map of the environment, en-

couraging the agent to explore new states, thus discovering the high-reward states. With eFeX, we make this exploration more efficient, and crucially, able to handle aliased states, thereby expanding its applicability. Furthermore, this immediately endows agents with the aforementioned functionalities, such as planning.

References

S. Amin, M. Gomrokchi, H. Satija, H. van Hoof, and D. Precup. A survey of exploration methods in reinforcement learning. *arXiv preprint arXiv:2109.00157*, 2021.

C. Beattie, J. Z. Leibo, D. Teplyashin, T. Ward, M. Wainwright, H. Küttler, A. Lefrancq, S. Green, V. Valdés, A. Sadik, et al. Deepmind lab. *arXiv preprint arXiv:1612.03801*, 2016.

M. Bellemare, S. Srinivasan, G. Ostrovski, T. Schaul, D. Saxton, and R. Munos. Unifying count-based exploration and intrinsic motivation. *Advances in neural information processing systems*, 29, 2016.

R.-D. Buhai, Y. Halpern, Y. Kim, A. Risteski, and D. Sontag. Empirical study of the benefits of overparameterization in learning latent variable models. In *International Conference on Machine Learning*, pages 1211–1219. PMLR, 2020.

A. K. Chandra, P. Raghavan, W. L. Ruzzo, and R. Smolensky. The electrical resistance of a graph captures its commute and cover times. In *Proceedings of the twenty-first annual ACM symposium on Theory of computing*, STOC ’89, pages 574–586, New York, NY, USA, Feb. 1989. Association for Computing Machinery. ISBN 9780897913072. doi: 10.1145/73007.73062. URL <https://doi.org/10.1145/73007.73062>.

H. Dai, Y. Li, C. Wang, R. Singh, P.-S. Huang, and P. Kohli. Learning transferable graph exploration. *Advances in Neural Information Processing Systems*, 32, 2019.

A. Ecoffet, J. Huizinga, J. Lehman, K. O. Stanley, and J. Clune. First return, then explore. *Nature*, 590(7847):580–586, Feb. 2021. ISSN 0028-0836, 1476-4687. doi: 10.1038/s41586-020-03157-9. URL <http://dx.doi.org/10.1038/s41586-020-03157-9>.

D. George, R. V. Rikhye, N. Gothoskar, J. S. Guntupalli, A. Dedieu, and M. Lázaro-Gredilla. Clone-structured graph representations enable flexible learning and vicarious evaluation of cognitive maps. *Nature communications*, 12(1):1–17, 2021.

R. Lambiotte, M. Rosvall, and I. Scholtes. From networks to optimal higher-order models of complex systems. *Nature physics*, 15(4):313–320, 2019.

M. C. Machado, M. G. Bellemare, and M. Bowling. A laplacian framework for option discovery in reinforcement learning. In *International Conference on Machine Learning*, pages 2295–2304. PMLR, 2017a.

M. C. Machado, C. Rosenbaum, X. Guo, M. Liu, G. Tesauro, and M. Campbell. Eigenoption discovery through the deep successor representation. *arXiv preprint arXiv:1710.11089*, 2017b.

A. K. McCallum. *Reinforcement learning with selective perception and hidden state*. University of Rochester, 1996.

I. Osband, C. Blundell, A. Pritzel, and B. Van Roy. Deep exploration via bootstrapped dqn. *Advances in neural information processing systems*, 29, 2016.

S. Ritter, R. Faulkner, L. Sartran, A. Santoro, M. Botvinick, and D. Raposo. Rapid task-solving in novel environments. *arXiv preprint arXiv:2006.03662*, 2020.

Shani and Brafman. Resolving perceptual aliasing in the presence of noisy sensors. *Advances in neural information processing systems*, 2004. ISSN 1049-5258. URL <https://proceedings.neurips.cc/paper/2004/file/c315f0320b7cd4ec85756fac52d78076-Paper.pdf>.

V. Sharan, S. M. Kakade, P. S. Liang, and G. Valiant. Learning overcomplete hmms. *Advances in Neural Information Processing Systems*, 30, 2017.

P. Shyam, W. Jaśkowski, and F. Gomez. Model-based active exploration. In *International conference on machine learning*, pages 5779–5788. PMLR, 2019.

A. L. Strehl and M. L. Littman. An analysis of model-based interval estimation for markov decision processes. *Journal of Computer and System Sciences*, 74(8):1309–1331, Dec. 2008. ISSN 0022-0000. doi: 10.1016/j.jcss.2007.08.009. URL <https://www.sciencedirect.com/science/article/pii/S0022000008000767>.

H. Tong, B. A. Prakash, T. Eliassi-Rad, M. Faloutsos, and C. Faloutsos. Gelling, and melting, large graphs by edge manipulation. In *Proceedings of the 21st ACM international conference on Information and knowledge management*, pages 245–254, 2012.

S. D. Whitehead and D. H. Ballard. Learning to perceive and act by trial and error. *Machine learning*, 7(1):45–83, July 1991. ISSN 0885-6125, 1573-0565. doi: 10.1007/BF00058926. URL <https://doi.org/10.1007/BF00058926>.

J. C. Whittington, T. H. Muller, S. Mark, G. Chen, C. Barry, N. Burgess, and T. E. Behrens. The tolman-eichenbaum machine: unifying space and relational memory through generalization in the hippocampal formation. *Cell*, 183(5):1249–1263, 2020.

H. S. Wilf. The editor’s corner: The white screen problem. *The American mathematical monthly: the official journal of the Mathematical Association of America*, 96(8):704–707, 1989. ISSN 0002-9890, 1930-0972. doi: 10.2307/2324718. URL <http://www.jstor.org/stable/2324718>.

J. Xu, T. L. Wickramarathne, and N. V. Chawla. Representing higher-order dependencies in networks. *Science advances*, 2(5):e1600028, 2016.

J. Xu, D. J. Hsu, and A. Maleki. Benefits of over-parameterization with em. *Advances in Neural Information Processing Systems*, 31, 2018.

T. Yang, H. Tang, C. Bai, J. Liu, J. Hao, Z. Meng, and P. Liu. Exploration in deep reinforcement learning: a comprehensive survey. *arXiv preprint arXiv:2109.06668*, 2021.

A. Model visualizations and degeneracy

Figure 4(a) shows two examples of latent graphs of the type considered in this work, where edges are labeled with both the action that makes the agent traverse them and the probability of that specific edge being traversed. As expected, outgoing edges under the same action sum up to one. The two graphs in this example are degenerate by a mechanism of *clone splitting*, as explained in Section 2.2 of the main paper. They are equivalent except for the red node, which is split into two separate red nodes in one of the graphs. Both graphs are equivalent under the expected log-likelihood, and indistinguishable if we only have access to their generated observations.

Figure 4(b) illustrates the data structures that represent the split CSCG, a transition matrix that defines the dynamics (one per action), and a (binary) emission matrix that defines the clone allocations.

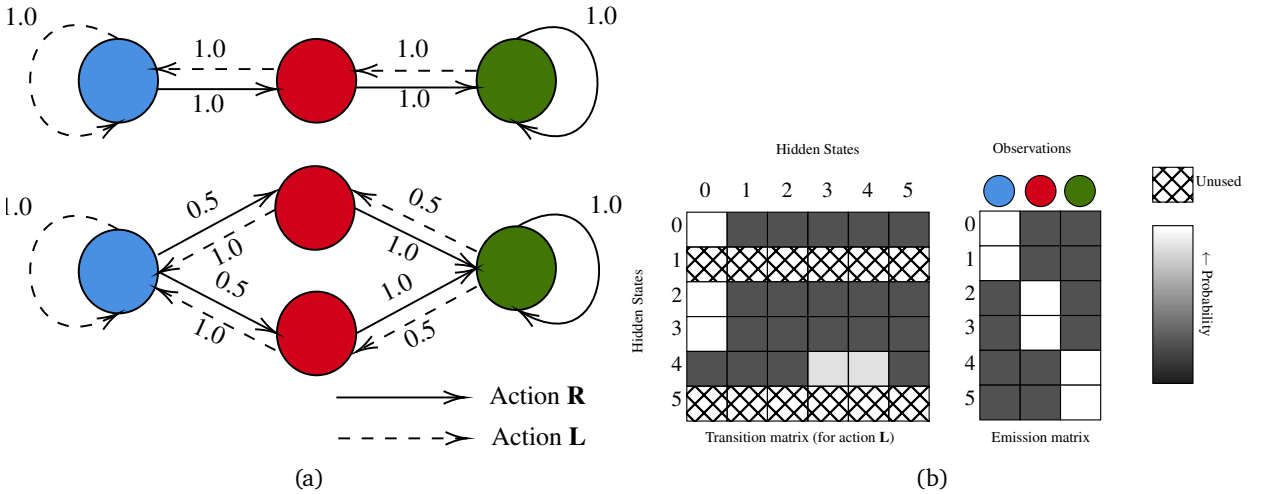


Figure 4 | (a) Latent graphs with two actions (L, R). The numbers on each edge are the probability of the edge given the state, action. The colors denote the observations. Note that both graphs will produce the same observations for any sequence of actions.

(b) Transition matrix (action left) and emission matrix for a CSCG representation of the bottom graph with two clones per observation.

B. eFeX Algorithm

This is the full pseudocode of the eFeX algorithm, described in Section 3 of the main paper. Figure 5 shows a visualization of the algorithm, where the utility of each node after a partial exploration is represented by the node size.

C. Performance measures

Here we introduce additional performance measures that are appropriate when working in environments with aliasing and stochasticity. Results for all performance measures under different topologies and parameterizations are reported in Appendix F.

Expected log-likelihood The performance should show how well G recovers the ground truth G' , and can be measured in different ways. An appealing choice is to simply use the expected log-likelihood $\mathcal{L}_{G'}(G)$, which does not require access to the ground truth latent states. This is an information-theoretic

Algorithm 1 Efficient exploration (eFeX) for aliased latent graph recovery

Input Discount factor γ , Dirichlet prior α , clone allocation E of size $n_E \times n_H$, number of exploration steps N .

Output Latent graph in tensor format T .

```

1:  $\mathcal{D}_0 \leftarrow (x_1,)$                                 ▷ Init sequence of observations
2:  $v \leftarrow U[0, 1]^{n_H}$                             ▷ Init all  $n_H$  entries randomly between 0 and 1
3:  $\hat{z}_1 \leftarrow \text{choice}(C(x_1))$                 ▷ Init  $z_1$  to a random clone of  $x_1$ 
4:  $c_{az} \leftarrow 0, \forall_{az}$                       ▷ Init  $c_{az}$  to a vector of  $n_H$  zeros
5: for  $n$  in  $1, \dots, N$  do
6:    $b_{az} \leftarrow c_{az} + \alpha, \forall_{az}$           ▷ Compute utility using (2)
7:    $u(z, a) = \text{utility}(b_{az}), \forall_{az}$         ▷ Compute mean transition tensor
8:    $\bar{t}_{az} \leftarrow b_{az}/1^\top b_{az}, \forall_{az}$ 
9:   repeat
10:    for  $z$  in  $1, \dots, n_H$  do
11:       $[v]_z \leftarrow \max_a \bar{t}_{az}^\top ((1 - \gamma)u(z, a) + \gamma v)$     ▷ Run value-iteration
12:    end for
13:   until convergence of  $v$ 
14:    $[\pi]_{\hat{z}_n} = \arg \max_a \bar{t}_{az}^\top ((1 - \gamma)u(z, a) + \gamma v)$     ▷ Recover optimal policy  $\pi$ 
15:    $a_n \leftarrow [\pi]_{z_n}$ 
16:    $x_{n+1} \leftarrow \text{Execute}(a_n)$           ▷ Take approximate best action, receive observation
17:    $\mathcal{D}_n \leftarrow \mathcal{D}_{n-1} \cup (a_n, x_{n+1})$     ▷ Grow sequence of observations
18:   Use EM to obtain the transition tensor  $T$  from  $\mathcal{D}_n$  (with pseudocount  $\alpha$ )
19:   Use Viterbi with  $T$  and  $E$  on  $\mathcal{D}_n$  to obtain a decoding  $\hat{z}_1, \dots, \hat{z}_{n+1}$ 
20:   Use  $\hat{z}_1, a_1 \dots, a_n, \hat{z}_{n+1}$  to compute  $c_{az}, \forall_{az}$ 
21: end for

```

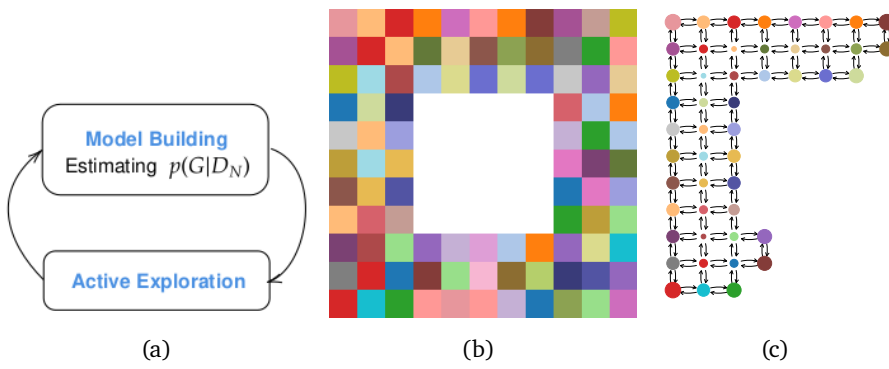


Figure 5 | (a) The algorithm alternates between estimating a distribution over beliefs given the observed data $p(G|\mathcal{D}_N)$ and using that distribution to decide which action to take next (active exploration) (b) Ground truth environment (c) Learned partial graph, with node size scaled according to the utility, $\max_a u(z, a)$ for each node z .

measure, upper bounded by $\mathcal{L}_{G'}(G')$, where $-\mathcal{L}_{G'}(G')$ is the entropy of the observations in the latent graph under a random policy. However, this measure is not very intuitive nor conveys how much of the graph has been recovered. To this end we define two additional, more easily interpretable measures.

Weighted coverage To assess whether an active policy Π (such as the dynamic policy in eFeX) is efficiently exploring a latent graph G' , we will want to measure how fast new edges of G' are being traversed as we take more exploration steps. We define the weighted coverage as follows

$$\text{WCOV}_{G'}(\Pi, N) = \frac{\sum_{n=1}^N P_{G'}(z_{n+1}|z_n, a_n) \mathbb{1}[(z_n^{(G')}, a_n, z_{n+1}^{(G')}) \neq (z_k^{(G')}, a_k, z_{k+1}^{(G')}) \forall k < n]}{\sum_{i,j,k} P_{G'}(z_{n+1} = k | z_n = j, a_n = i)}, \quad (3)$$

where the indicator function $\mathbb{1}[\cdot]$ evaluates to 1 if the expression inside the brackets is true and to 0 otherwise. The numerator iterates over the ground truth triplets $(z_n^{(G')}, a_n, z_{n+1}^{(G')})$ that define the edge of G' that is being traversed at time step n according to the policy Π , accumulating the probabilistic weight of that edge. The term in the indicator function ensures that each edge is only counted once, the first time that it is visited. The denominator sums the weight of all edges in G' , thus returning a normalized weighted coverage. This measure will only reach a value of 1 once all the edges in the ground truth graph G' have been visited. Low-probability edges have a smaller impact in this measure.

Observe that $\text{WCOV}_{G'}(\Pi, N)$ only tells us how good eFeX (or any other algorithm) is at providing an efficient exploration policy Π for G' , but does not tell us how good the exploration algorithm is in terms of recovering G' . In fact, this measure can be used with algorithms that do not have an explicit model G that attempts to recover G' . Thus, we complement this measure with another one that focuses on the quality of the model G , the *precision*.

Precision If a model G has recovered a good approximation of the unobservable latent graph G' , the hidden states of G should map well to the latent states of G' . As discussed in Section 2.2, G might contain several “split” hidden states that map to the same latent state of G' , and this degenerate solution can still be perfect in terms of modeling G' . Thus, a way to assess the quality of a model given a sequence of latent ground truth states $\{z_n^{(G')}\}_{n=1}^N$ and the corresponding sequence of hidden states $\{\hat{z}_n^{(G)}\}_{n=1}^N$ estimated by the model G from observations $\{x_n, a_n\}_{n=1}^N$, is to measure *the accuracy of a predictor that uses the best fixed mapping* from each estimated state $\hat{z}_n^{(G)}$ to each ground truth state $z_n^{(G')}$. Mathematically, we define this precision for the case of an infinitely long walk under a uniform random policy,

$$\text{PREC}_{G'}(G) = \lim_{N \rightarrow \infty} \mathbb{E}_{a_1, \dots, a_N \sim \mathcal{U}} \left\{ \frac{1}{N} \sum_i \max_j \sum_n \mathbb{1}[\hat{z}_n^{(G)} = i] \mathbb{1}[z_n^{(G')} = j] \right\}. \quad (4)$$

Observe that this measure penalizes models that estimate the same hidden state for multiple different ground truth latent states (since each hidden state from the model G can only be mapped to a single latent state from the ground truth G' , all the other latent states will register as errors and reduce the accuracy of the predictor). Conveniently, this measure does not penalize degenerate solutions: having multiple “split” hidden states map to the same ground truth latent state will still not incur in any prediction errors. Thus, perfect degenerate solutions should have a precision of 1, with smaller values implying that the recovered G is conflating more than one latent state from G' into the same hidden state in G .

In our experiments, we will approximate the precision by performing 100 walks starting at random locations of 10,000 steps each, and computing $\{\hat{z}_n^{(G)}\}_{n=1}^N$ from the obtained walk data $\{x_n, a_n\}_{n=1}^N$

using Viterbi decoding. The same walk data (without Viterbi decoding) are used to approximately evaluate the expected log-likelihood.

D. Topologies

The topologies that we test are shown in Figure 3 (bottom), with each color representing a different observation. In detail (from left to right in the figure):

Regular grids A $7 \times 7 \times 7$ 3D grid (not shown) and a 21×21 2D grid. With respectively 6 and 4 actions, allowing the agent to traverse to the adjacent cells (and further due to slippage). Boundaries contain self-loops, so the agent will remain in place when attempting to exit the topology. These structures do not contain obstacles or bottlenecks that hinder exploration, so a random policy will explore them fairly quickly, although it might struggle to capture the last few nodes.

Interconnected grids (ICG) Four 2D grids of size 10×10 connected by corridors of length 3. Each grid forms a cluster of highly connected nodes, whereas connecting across grids is more challenging. These are similar to “lollipop” graphs discussed in (Chandra et al., 1989) which, as noted in the reference, mimic real world connectivity patterns. Such graphs require the agent to deliberately go through the corridors in order to get to different parts of the graph. Boundaries are self-looped as above.

Dense maze Dense mazes are generated by running a depth-first search on a 2D grid, and then up-sampling it by a factor of five to make the corridors five times as thick as the walls, with the final result being a 21×21 grid with gaps. Boundaries are self-looped. These mazes demand that the agent performs long sequences of suitably correlated actions to fully recover the environment, which in turn necessitate a good model of how the environment explored so far reacts to actions. Boundaries are self-looped as above.

Sparse maze Sparse mazes are generated on a background of size 21×21 using the open source “lab-maze” library introduced in Beattie et al. (2016). Boundaries are self-looped as above.

E. Derivation of Utility

In this section we provide the derivation for our expression to compute utility:

$$u(z, a) = H\left(\frac{b_{az}}{1^\top b_{az}}\right) + \left(\frac{1^\top (b_{az} \odot \psi(b_{az} + 1))}{1^\top b_{az}}\right) - \psi(1^\top b_{az} + 1),$$

With begin with Equation 2:

$$u(z, a) = H(\mathbb{E}_{t_{az} \sim \text{Dir}(b_{az})}[t_{az}]) - \mathbb{E}_{t_{az} \sim \text{Dir}(b_{az})}[H(t_{az})]. \quad (5)$$

For convenience, we drop the subscript za for this proof and write the utility u of a particular state z and action a pair as:

$$u = H(\mathbb{E}_{t \sim \text{Dir}(b)}[t]) - \mathbb{E}_{t \sim \text{Dir}(b)}[H(t)], \quad (6)$$

where t is the distribution $p(z'|z, a)$ and b is the vector that parameterizes the $K+1$ dimensional Dirichlet distribution over t (assuming $K+1$ states $z_{0:K}$).

The above equation has two components which we analyze separately. The first component is the entropy of the expected transition distribution t . Since $t \sim \text{Dir}(b)$, we know that:

$$\mathbb{E}_{t \sim \text{Dir}(b)}[t] = \frac{b}{\sum_i b[i]}, \quad (7)$$

which can be alternatively written as

$$\mathbb{E}_{t \sim \text{Dir}(b)}[t] = \frac{b}{1^\top b}. \quad (8)$$

Now we move to the second term, which is $\mathbb{E}_{t \sim \text{Dir}(b)}[H(t)]$. For a particular sample $t = (t_0, t_1, \dots, t_K)$, the entropy $H(t)$ can be written as:

$$H(t) = - \sum_{i=0}^K t_i \log t_i. \quad (9)$$

Then,

$$\mathbb{E}_{t \sim \text{Dir}(b)}[H(t)] = - \int_{t \sim \text{Dir}(b)} p(t) \sum_{i=0}^K t_i \log t_i dt \quad (10)$$

$$= - \sum_{i=0}^K \int_{t \sim \text{Dir}(b)} p(t) t_i \log t_i dt. \quad (11)$$

We can re-write the previous equation as

$$\mathbb{E}_{t \sim \text{Dir}(b)}[H(t)] = - \sum_{i=0}^K x_i \quad (12)$$

where x_i is defined as:

$$x_i = \int_{t \sim \text{Dir}(b)} p(t) t_i \log t_i dt. \quad (13)$$

Using the definition of the Dirichlet distribution to expand Equation 13 we get:

$$x_i = \frac{1}{B(b)} \int_{0 \leq t_0 \leq \dots \leq t_K \leq 1, \sum_i t_i = 1} \prod_j t_j^{b_j-1} t_i \log t_i dt_{0:K}, \quad (14)$$

where $B(\cdot)$ is the Beta function, and the integral is over the simplex over t . To further analyze the above equation, we need to look at the definition of the Beta function:

$$B(b) = \int_{0 \leq t_0 \leq \dots \leq t_K \leq 1, \sum_i t_i = 1} \prod_j t_j^{b_j-1} dt_{0:K}. \quad (15)$$

Notice the derivative of $B(b)$ w.r.t b_i :

$$\frac{\partial B(b)}{\partial b_i} = \int_{0 \leq t_0 \leq \dots \leq t_K \leq 1, \sum_i t_i = 1} \prod_{j \neq i} t_j^{b_j-1} t_i^{b_i-1} \log t_i dt_{0:K}. \quad (16)$$

If I_i is a one-hot $K+1$ dimensional vector which is 0 everywhere and 1 at index i , then we can write x_i as:

$$x_i = \frac{1}{B(b)} \frac{\partial B(b + I_i)}{\partial b_i}. \quad (17)$$

The derivative of the Beta function is a well known quantity:

$$\frac{\partial B(b + I_i)}{\partial b_i} = B(b + I_i) \left(\psi(b_i + 1) - \psi(1 + \sum_j b_j) \right), \quad (18)$$

where $\psi(\cdot)$ is the polygamma function. Using this expansion we have:

$$x_i = \frac{B(b + I_i)}{B(b)} \left(\psi(b_i + 1) - \psi(1 + \sum_j b_j) \right). \quad (19)$$

Using the alternative definition of $B(b)$ in terms of the gamma function

$$B(b) = \frac{1}{\Gamma(\sum_j b_j)} \prod_i \Gamma(b_i), \quad (20)$$

we get:

$$\frac{B(b + I_i)}{B(b)} = \frac{\Gamma(b_i + 1) \Gamma(\sum_j b_j)}{\Gamma(b_i) \Gamma(1 + \sum_j b_j)}. \quad (21)$$

The gamma function has the property that $\Gamma(x + 1) = x\Gamma(x)$, which simplifies the above expression as:

$$\frac{B(b + I_i)}{B(b)} = \frac{b_i}{\sum_j b_j}. \quad (22)$$

Substituting Equation 22 in Equation 19, we have:

$$x_i = \frac{B(b + I_i)}{B(b)} = \frac{b_i}{\sum_j b_j} \left(\psi(b_i + 1) - \psi(1 + \sum_j b_j) \right). \quad (23)$$

Combining Equations 23 and 12 we have:

$$\mathbb{E}_{t \sim \text{Dir}(b)} [H(t)] = - \sum_{i=0}^K \frac{b_i}{\sum_j b_j} \left(\psi(b_i + 1) - \psi(1 + \sum_j b_j) \right), \quad (24)$$

which further simplifies to

$$\mathbb{E}_{t \sim \text{Dir}(b)} [H(t)] = \psi(1 + \sum_j b_j) - \sum_{i=0}^K \frac{b_i}{\sum_j b_j} \left(\psi(b_i + 1) \right). \quad (25)$$

Re-writing the sum as a dot product we get:

$$\mathbb{E}_{t \sim \text{Dir}(b)} [H(t)] = \psi(1 + \mathbf{1}^\top b) - \mathbf{1}^\top \left(\frac{b \odot \psi(b + 1)}{\mathbf{1}^\top b} \right). \quad (26)$$

Equation 8 and Equation 26 can be substituted into Equation 6 to get

$$u = H \left(\frac{b}{\mathbf{1}^\top b} \right) + \left(\frac{\mathbf{1}^\top (b \odot \psi(b + 1))}{\mathbf{1}^\top b} \right) - \psi(1^\top b + 1),$$

which completes the proof.

F. Additional experiments

F.1. Parameters: $UF = 1.0$ and $P_{\text{slip}} = 0.00$

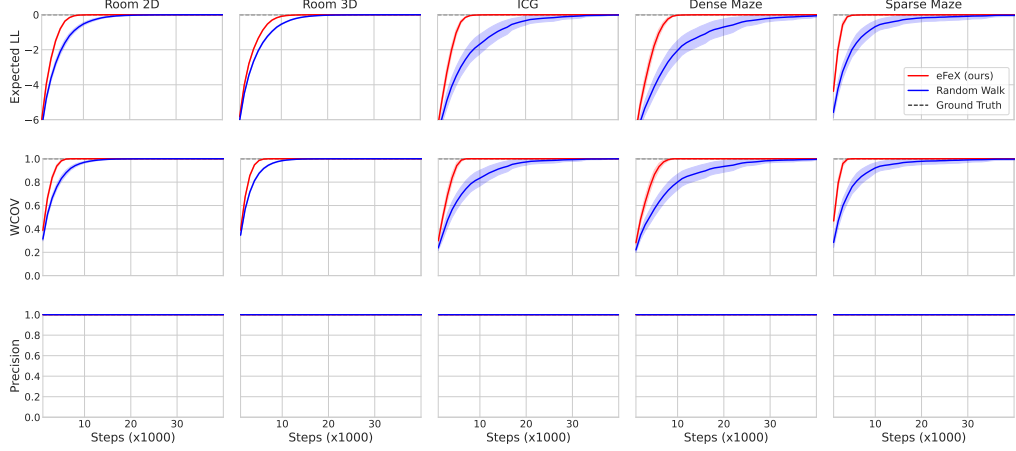


Figure 6 | Expected log-likelihood, weighted coverage, and precision, for each topology, as a function of the number of steps of the agent in the environment. See Appendix C for further explanation. Higher is better. Results are averaged over 100 runs. Bands indicate 95% confidence intervals for the averages. Random policy shown in blue, eFeX in red.

F.2. Parameters: $UF = 1.0$ and $P_{\text{slip}} = 0.01$

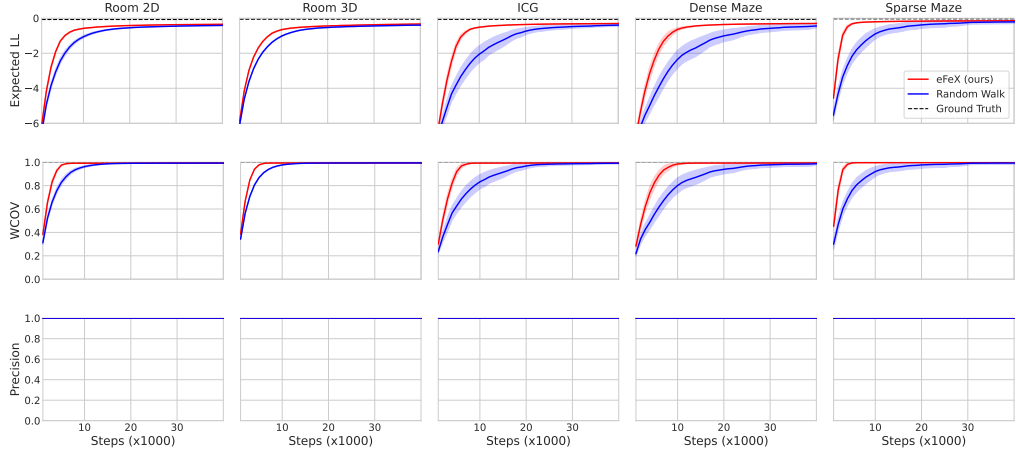


Figure 7 | Expected log-likelihood, weighted coverage, and precision, for each topology, as a function of the number of steps of the agent in the environment. See Appendix C for further explanation. Higher is better. Results are averaged over 100 runs. Bands indicate 95% confidence intervals for the averages. Random policy shown in blue, eFeX in red.

F.3. Parameters: $UF = 1.0$ and $P_{\text{slip}} = 0.10$

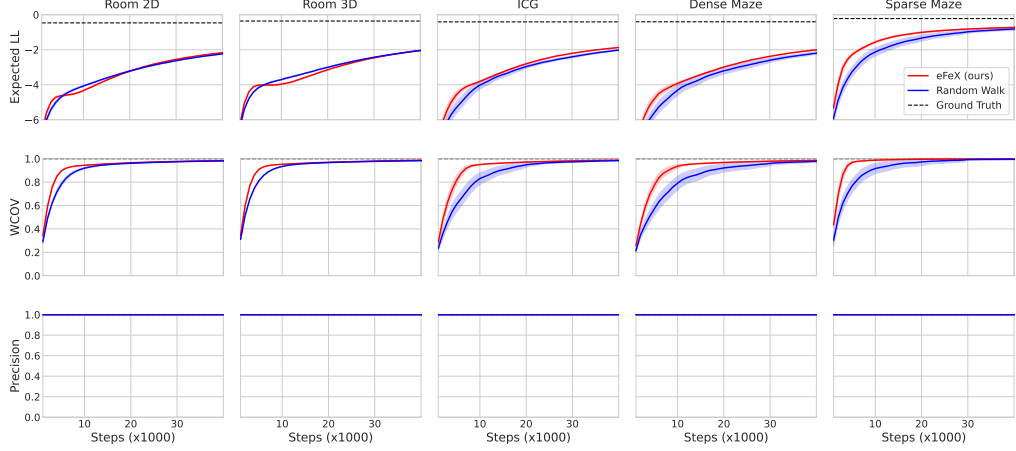


Figure 8 | Expected log-likelihood, weighted coverage, and precision, for each topology, as a function of the number of steps of the agent in the environment. See Appendix C for further explanation. Higher is better. Results are averaged over 100 runs. Bands indicate 95% confidence intervals for the averages. Random policy shown in blue, eFeX in red.

F.4. Parameters: $UF = 0.3$ and $P_{\text{slip}} = 0.00$

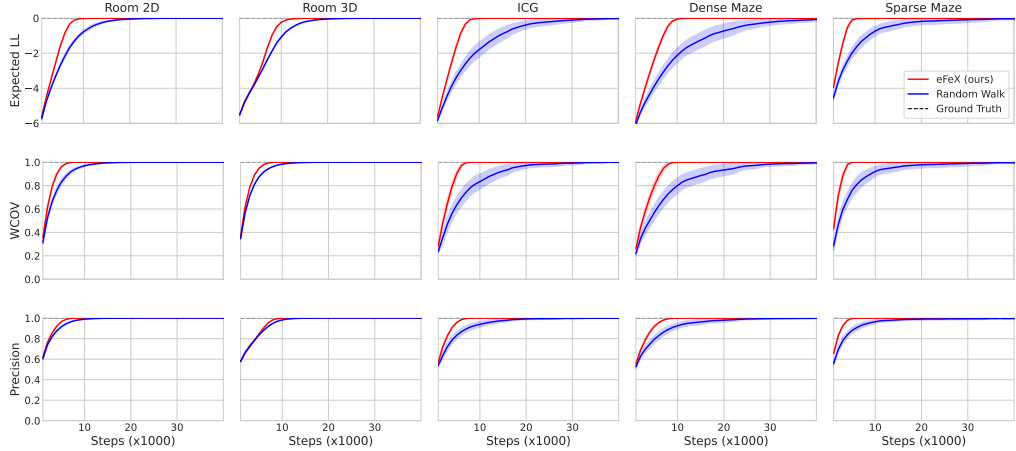


Figure 9 | Expected log-likelihood, weighted coverage, and precision, for each topology, as a function of the number of steps of the agent in the environment. See Appendix C for further explanation. Higher is better. Results are averaged over 100 runs. Bands indicate 95% confidence intervals for the averages. Random policy shown in blue, eFeX in red.

F.5. Parameters: $UF = 0.3$ and $P_{\text{slip}} = 0.01$

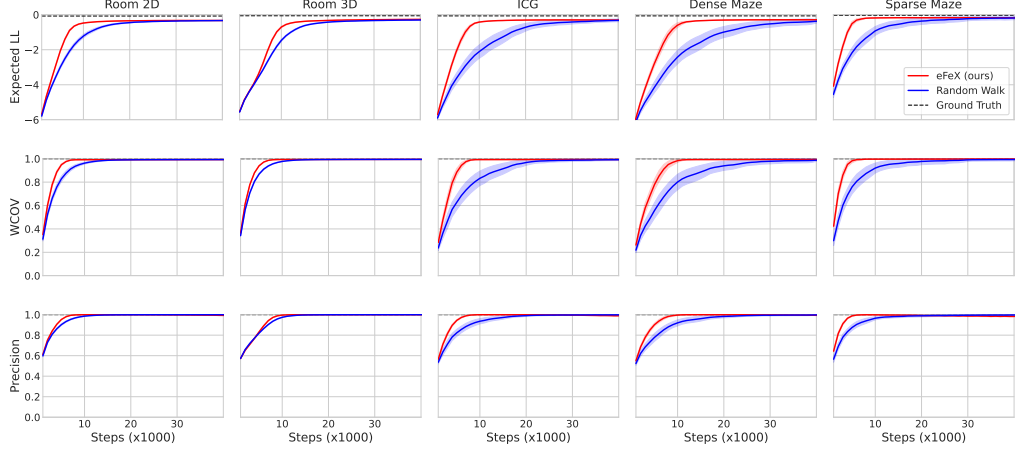


Figure 10 | Expected log-likelihood, weighted coverage, and precision, for each topology, as a function of the number of steps of the agent in the environment. See Appendix C for further explanation. Higher is better. Results are averaged over 100 runs. Bands indicate 95% confidence intervals for the averages. Random policy shown in blue, eFeX in red.

F.6. Parameters: $UF = 0.3$ and $P_{\text{slip}} = 0.10$

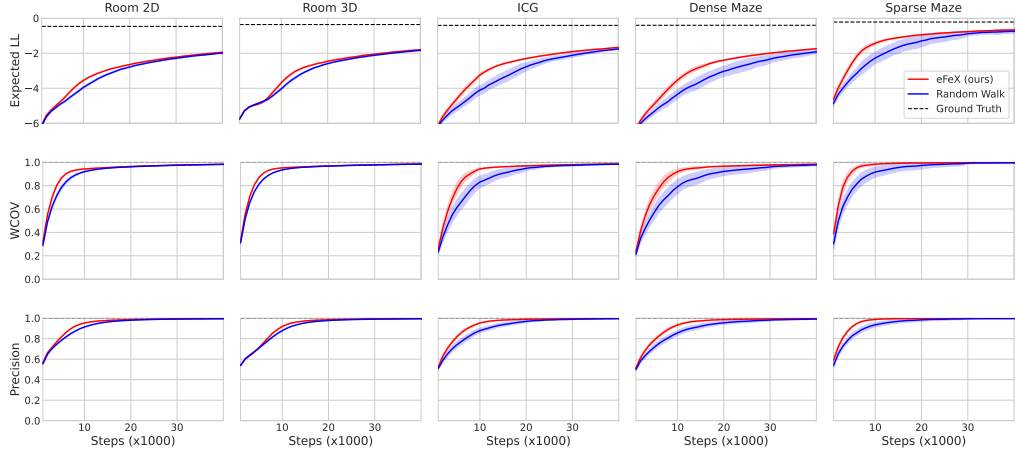


Figure 11 | Expected log-likelihood, weighted coverage, and precision, for each topology, as a function of the number of steps of the agent in the environment. See Appendix C for further explanation. Higher is better. Results are averaged over 100 runs. Bands indicate 95% confidence intervals for the averages. Random policy shown in blue, eFeX in red.

F.7. Parameters: $UF = 0.1$ and $P_{\text{slip}} = 0.00$

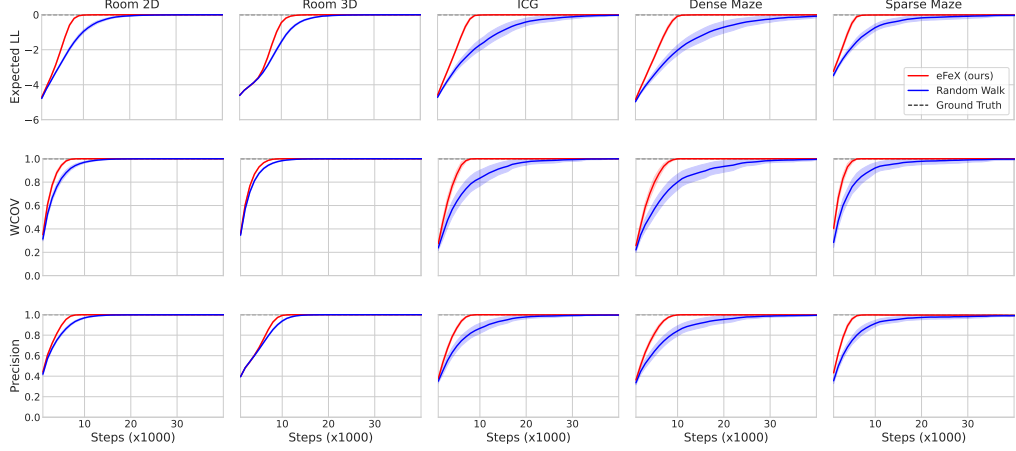


Figure 12 | Expected log-likelihood, weighted coverage, and precision, for each topology, as a function of the number of steps of the agent in the environment. See Appendix C for further explanation. Higher is better. Results are averaged over 100 runs. Bands indicate 95% confidence intervals for the averages. Random policy shown in blue, eFeX in red.

F.8. Parameters: $UF = 0.1$ and $P_{\text{slip}} = 0.01$

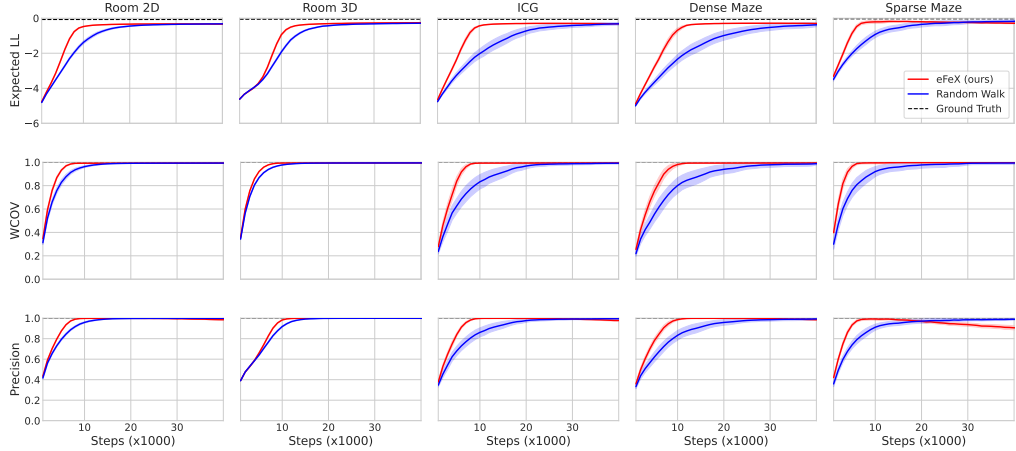


Figure 13 | Expected log-likelihood, weighted coverage, and precision, for each topology, as a function of the number of steps of the agent in the environment. See Appendix C for further explanation. Higher is better. Results are averaged over 100 runs. Bands indicate 95% confidence intervals for the averages. Random policy shown in blue, eFeX in red.

F.9. Parameters: $UF = 0.1$ and $P_{\text{slip}} = 0.10$

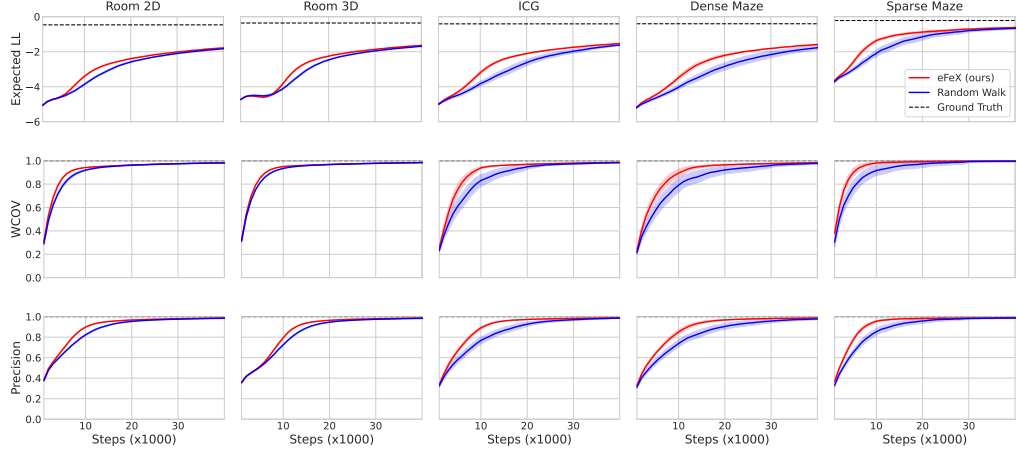


Figure 14 | Expected log-likelihood, weighted coverage, and precision, for each topology, as a function of the number of steps of the agent in the environment. See Appendix C for further explanation. Higher is better. Results are averaged over 100 runs. Bands indicate 95% confidence intervals for the averages. Random policy shown in blue, eFeX in red.